ELSEVIER

Chemical Geology 236 (2007) 323–338

CHEMICAL GEOLOGY
INCLUDING
ISOTOPE GEOSCIENCE

www.elsevier.com/locate/chemgeo

Re–Os evidence for the age and origin of peridotites from the Dabie–Sulu ultrahigh pressure metamorphic belt, China

Honglin Yuan[a,b], Shan Gao[a,b,*], Roberta L. Rudnick[c], Zhenmin Jin[b], Yongsheng Liu[b], Igor S. Puchtel[c], Richard J. Walker[c], Ridong Yu[b]

[a] *State Key Laboratory of Continental Dynamics, Department of Geology, Northwest University, Xi'an, 710069, China*
[b] *State Key Laboratory of Geological Processes and Mineral Resources, Faculty of Earth Sciences, China University of Geosciences, 430074, China*
[c] *Geochemistry Laboratory, Department of Geology, University of Maryland, College Park, MD 20742, USA*

Received 29 April 2006; received in revised form 24 September 2006; accepted 15 October 2006

Editor: S.L. Goldstein

Abstract

Serpentinized garnet peridotites from the Xugou peridotite body of the Sulu ultrahigh-pressure (UHP) metamorphic terrane, central eastern China, are refractory (olivines have $Fo_{91.7–93.1}$), indicating their origin as residual mantle. Negative correlations between whole-rock MgO and TiO_2, Al_2O_3, total Fe_2O_3 and CaO ($r=-0.90$ to -0.95) and positive correlations between whole-rock Al_2O_3 and CaO and incompatible elements [Li, V, Cu, Ga, Sr, Y, Zr, heavy rare earth elements (HREEs), Hf, Pb and U] ($r=0.69$ to 0.98) likely reflect melt depletion trends. Four highly refractory samples were selected for Re–Os isotopic analysis. Although they show evidence of variable enrichment of incompatible elements during serpentinization/metasomatism, no correlations exist between $^{187}Re/^{188}Os$ or $^{187}Os/^{188}Os$ with either La or Re ($r=0.00$ to 0.17). These results indicate that any Re addition was fairly recent and did not affect the Os isotopic composition significantly. The correlation between $^{187}Os/^{188}Os$ and $^{187}Re/^{188}Os$ ratios thus, most likely reflects an ancient melt extraction event.

The T_{RD}, T_{MA} and errorchron ages of the Xugou peridotites are all similar, suggesting that these peridotites formed around 2.0 Ga ago. This age is similar to Os model ages of mantle peridotites from the Dabie terrane, but contrasts markedly with the Archean ages of the continental lithospheric mantle (CLM) beneath the eastern block of the North China craton (NCC). If we assume that the Dabie–Sulu belt formed by the Triassic collision of the Yangtze craton with the *eastern block* of NCC and that the Archean aged CLM of the latter persisted until the Triassic, the Paleoproterozoic ages suggest derivation of these Dabie–Sulu mantle peridotites from the Yangtze craton. A Yangtze craton origin is consistent with the existing tectonic model of the Dabie–Sulu UHP belt. Our results support the hypothesis that the crust and underlying lithospheric mantle of the Yangtze craton were subducted to depths of >180–200 km to form the world's largest UHP belt.

Keywords: Re–Os isotopes; Dabie–Sulu; Eastern China; CLM

1. Introduction

The Re–Os isotopic system is currently the most robust method for dating the formation of the continental

* Corresponding author. State Key Laboratory of Continental Dynamics, Department of Geology, Northwest University, Xi'an, 710069, China.
E-mail address: sgao@263.net (S. Gao).

0009-2541/$ - see front matter © 2006 Elsevier B.V. All rights reserved.
doi:10.1016/j.chemgeo.2006.10.009

lithospheric mantle, CLM (Walker et al., 1989; Pearson, 1999; Lee et al., 2000; Pearson et al., 2003; Carlson et al., 2005). During melting of peridotites, Re is moderately incompatible and Os is strongly compatible, so that the Re/Os ratio of the residue is lowered by melt extraction and radiogenic Os in-growth is retarded relative to convecting mantle. Re–Os systematics can, thus, be used to date lithospheric mantle formation. Moreover, despite some shift in Re and Os concentrations due to sulfide metasomatism in some peridotites (Chesley et al., 1999; Alard et al., 2000), whole-rock Os isotopic compositions are relatively immune to disturbance through metasomatism, due to the low Os concentrations in infiltrating silicate melts relative to those in peridotites (Chesley et al., 1999; Reisberg et al., 2004; Carlson et al., 2005).

Peridotite xenoliths entrained in basalts and kimberlites and orogenic massif peridotites occurring in high-pressure (HP) and ultrahigh-pressure (UHP) metamorphic belts are both samples of the lithospheric mantle (Bodinier and Godard, 2003; Pearson et al., 2003). Re–Os isotopic studies of these mantle samples have provided significant insights into the timing of formation of the CLM and its relationship to the continental crust (Shirey and Walker, 1998; Pearson, 1999; Pearson et al., 2003; Carlson et al., 2005).

Numerous studies of eclogites and surrounding gneisses from the Dabie–Sulu UHP belt suggest that these rocks derive from the Yangtze craton and collectively experienced *in situ* UHP metamorphism during the Triassic (Li et al., 1993; Ye et al., 2000b; Hacker et al., 2000; Liu et al., 2004). Studies of peridotites and associated garnet pyroxenites in the Dabie–Sulu UHP belt have primarily been aimed at determining their origin (cumulate vs. residual upper mantle), their metamorphic (Zhang et al., 1994, 1995a,b; Zhang and Liou, 1998; Zhang et al., 2000; Yang and Jahn, 2000; Zhang et al., 2003; Zhang and Liou, 2003; Jahn et al., 2003; Yang, 2003; Zhang et al., 2005) and metasomatic histories (Zheng et al., 2005, 2006a,c). Metamorphic zircons from the Zhimafang mantle peridotite from pre-pilot hole PP1 of the Chinese Continental Scientific Drilling (CCSD) project in the Sulu terrane were dated by the SHRIMP U–Pb and LA-ICP-MS methods at 220–224 Ma (Zhang et al., 2005; Zheng et al., 2006a). This age is similar to the age of peak metamorphism of the eclogites (e.g., Ayers et al., 2002; Liu et al., 2004) and suggest that the peridotites were tectonically emplaced into a subducting crustal slab and subjected to *in situ* Triassic subduction zone UHP metamorphism (Zhang et al., 2003, 2005). Based on the refractory compositions and relatively unradiogenic Hf isotopic compositions of zircons from the Sulu garnet peridotites, Zheng et al. (2006a,c) suggest that they are fragments of refractory Archean mantle derived from the NCC that experienced Mesoproterozoic metasomatism. Jin et al. (2004) report Re–Os isotopic compositions of the Raobozhai mantle peridotites (including serpentinized harzburgite and dunite) from the Dabie terrane. From correlations between Os isotopes and Al_2O_3 and Yb contents, they derived initial $^{187}Os/^{188}Os$ ratios in the range from 0.1141 to 0.1164, which correspond to T_{RD} ages of 1800–2100 Ma. However, the age of melt depletion and provenance of the Sulu peridotites, as determined by Re–Os isotopes, have yet to be established. Their origins could be continental lithospheric mantle from the Yangtze craton, the North China craton (NCC) or Triassic mantle wedge peridotite.

Here, we report mineralogical, geochemical and Re–Os isotopic compositions of the mantle-derived Xugou serpentinized garnet peridotites from the Sulu terrane, which is 30 km northwest of the CCSD pre-pilot hole at Zhimafang (Fig. 1). Together with published data for the Dabie peridotites and peridotite xenoliths from the NCC, we discuss the age, origin and provenance of peridotites from the Dabie–Sulu orogenic belt.

2. Geologic setting and samples

The Dabie–Sulu orogenic belt, the world's largest UHP metamorphic belt, formed by Triassic subduction of the Yangtze craton beneath the NCC (Fig. 1). It is generally accepted that the belt is offset by the Tanlu Fault and displaced northward approximately 500 km to the Sulu terrane, which is adjacent to the eastern block of the NCC. Garnet peridotites occur as lenses, blocks or layers in the Dabie–Sulu UHP belt and are associated with coesite-bearing eclogite (e.g., Zhang et al., 1994; Zhang and Liou, 1998; Zhang et al., 2000, 2003, 2005; Zheng et al., 2005, 2006a,c). Zhang et al. (2000) divided garnet peridotites from the Dabie–Sulu belt into two types based on mode of occurrence and petrochemical characteristics. Type A is mantle-derived and originated from either: (1) the mantle wedge above a subduction zone, (2) the footwall mantle of the subducted slab, or (3) were ancient mantle fragments emplaced at crustal depths prior to UHP metamorphism. Type A peridotites are further subdivided into two subgroups: A-1, residual mantle fragments, and A-2, peridotite and pyroxenite, which differentiated from mantle-derived magma in the uppermost mantle. In contrast, type B peridotites have a crustal origin and formed as part of mafic–ultramafic cumulate complexes from magmas that intruded into the continental crust prior to subduction. Thus, type B peridotites do not represent true mantle rocks. Both type A and type B peridotites experienced UHP metamorphism

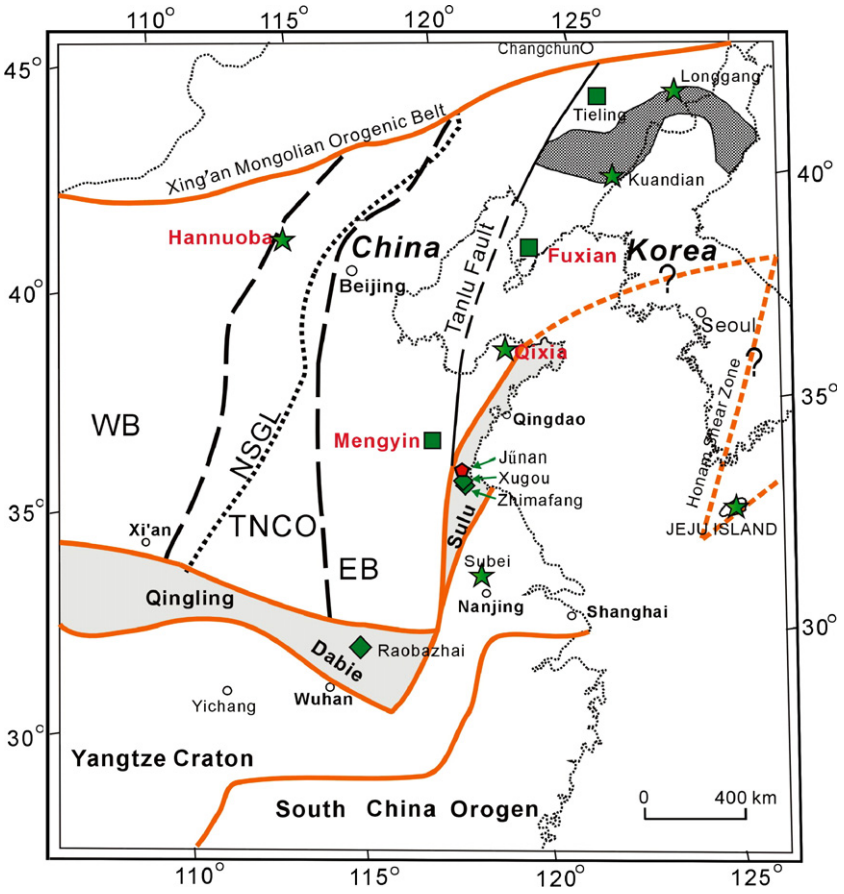

Fig. 1. Tectonic sketch map of central eastern China, showing the peridotite sample localities discussed in the study. Squares denote garnet peridotite xenoliths from Ordovician kimberlites (Gao et al., 2002; Wu et al., 2006; Zhang et al., 2006), pentagon represents peridotite xenoliths from the Late Cretaceous basaltic breccia (Ying et al., 2006), stars represent peridotite xenoliths from Cenozoic basalts (Gao et al., 2002; Wu et al., 2003; Reisberg et al., 2005; Wu et al., 2006; Lee and Walker, 2006), and diamonds indicate orogenic mantle peridotites at Raobozhai (Jin et al., 2004) in the Dabie terrane and at Xugou and Zhimafang in the Sulu terrane (Zhang and Liou, 1998; Zhang et al., 2000, 2003, 2005; Zheng et al., 2005, 2006a,c; this study). Also shown are the subdivisions of the North China craton (Zhao et al., 2001), where WB, TNCO and EB denote the Western Block, Trans-North China Orogen and Eastern Block, respectively. The Dabie–Sulu UHP belt is shown in light shading, and the Paleoproterozoic orogenic belt along the northern margin of the eastern block of the North China craton (Wu et al., 2006) is shown in darker gray. NSGL indicates the North–South Gravity Lineament (Griffin et al., 1998). The dashed line with question mark is the likely boundary of the North China craton in Korea (Lee and Walker, 2006).

during the Triassic collision between the North China and Yangtze cratons. Some of the peridotites record prograde histories. Peak P–T estimates of metamorphism (760–970 °C and 4.0–6.5±0.2 GPa) indicate that they were subducted to great depths >180–200 km along an extremely low geothermal gradient of <5 °C km^{-1} (Zhang et al., 2000).

Samples investigated here were collected from the Xugou garnet peridotite body, Donghai County, which is located at the southern end of the Sulu terrane (Fig. 1). The fault-bounded Xugou garnet peridotite body, which measures 1500×500 m and is enclosed in felsic gneiss, is dominated by serpentinized harzburgite with rare lherzolite (Zhang et al., 2003; Zheng et al., 2005, 2006c). Small lenses or layers of garnet–pyroxene rocks enclosed concordantly within the peridotites consist of both clinopyroxenite (Jd<20 mol%) and eclogite (Jd>20 mol%), ranging from 0.5 to 15 m in thickness. Based on their refractory whole-rock and mineral chemistry (Fig. 2), these peridotites are type A-1 according to Zhang et al.'s (2000, 2003) classification and are residual, mantle-derived peridotites. In contrast, protoliths of eclogite and garnet clinopyroxenite are interpreted to be cumulates from mantle-derived melt, containing variable amounts of trapped melt. Both garnet peridotites and associated eclogites/garnet clinopyroxenites experienced Triassic UHP metamorphism at 780–870 °C and 5–6.7 GPa in the "forbidden zone" of the P–T field [the P–T region with very low temperatures and high pressures, corresponding to an ultra-low geothermal gradient of

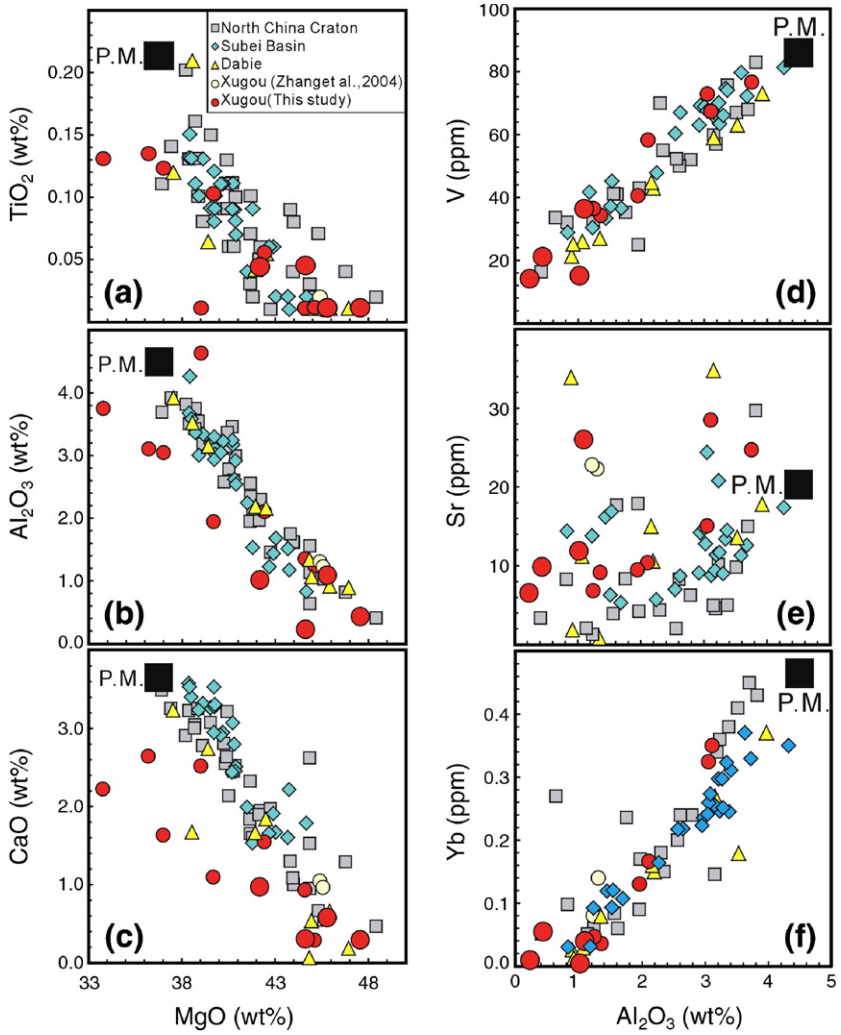

Fig. 2. Whole-rock MgO versus TiO_2 (a), Al_2O_3 (b), and CaO (c), and whole-rock Al_2O_3 versus V (d), Sr (e), and Yb (f) for the Xugou peridotites. Filled circles are samples from this work, large filled circles are the four highly depleted samples analyzed for Re–Os isotopic compositions. Open circles are Xugou peridotites from Zhang et al. (2003). Also shown for comparison are mantle peridotites from the Dabie terrane (triangles) (Jin et al., 2004) and peridotite xenoliths from North China craton (squares) [including Hannuoba and Qixia (Rudnick et al., 2004) and Longgang and Kuandian (Wu et al., 2003, 2006)] and from the Subei basin (diamonds) (Reisberg et al., 2005). PM denotes primitive mantle (Palme and O'Neill, 2003).

<5 °C km^{-1}; Liou et al., 2000; Zhang et al., 2003], and multistage retrograde metamorphism at granulite–amphibolite to greenschist facies conditions during exhumation (Zhang et al., 2003).

Here we focus on the garnet peridotites, which are partially to completely serpentinized and strongly deformed. Over twenty serpentinized garnet peridotites were collected, 11 of which were analyzed for major and trace element compositions. These peridotite samples have diameters ranging from 10–30 cm. Based on whole-rock and mineral chemistry, four highly depleted samples were selected for detailed mineralogical, chemical and Re–Os isotopic analyses, with the expectation that these samples are likely to provide the best constraints on the age, provenance and origin of the peridotites.

3. Analytical techniques

Major element compositions of minerals were analyzed at the Department of Geology, Peking University, using a JEOL Superprobe JXA 8100. The operating conditions were as follows: accelerating voltage 15 kV, beam current 1×10^{-8} A, and the spot size 1 μm.

The peridotites were crushed in an alumina jaw crusher and then ground to fine powder in an agate

mortar. Chemical compositions of whole rock samples were measured at the State Key Laboratory of Continental Dynamics, Northwest University. Major element compositions were analyzed by XRF in fused glass disks using a Rigaku RIX 2100 spectrometer. Trace element compositions were analyzed by ICP-MS (Agilent 7500a, Agilent Technologies, Wilmington, USA) after acid digestion of samples in Teflon bombs. Analyses of the USGS rock standards (BCR-2, BHVO-1 and AGV-1) indicate precision and accuracy better than 5% for major elements and 10% for trace and rare earth elements (see data in Rudnick et al., 2004).

Concentrations of Re and Os and Os isotopic compositions in the four peridotite samples were determined at the Isotope Geochemistry Laboratory, University of Maryland, using Carius tube (CT) digestion in combination with isotope dilution thermal ionization mass-spectrometry (ID-TIMS) and multiple collector inductively coupled plasma mass-spectrometry (ID-MC-ICP-MS) techniques, following the procedures of Walker et al. (2002, 2005). Approximately 2 g of rock powder, an appropriate amount of the Re–Os mixed spike, and ~9 mL of inverse *aqua regia* were placed into a chilled (0 °C) thick-walled Pyrex® borosilicate glass Carius tube, and sealed. The digestions were performed at ~250 °C for 48–72 h. After opening the tubes, Os was extracted from the *aqua regia* solution into CCl_4 (Cohen and Waters, 1996) and then back-extracted into HBr, followed by purification via microdistillation (Birck et al., 1997). The residual *aqua regia* solution was dried, and Re was separated from the matrix and further purified by anion exchange chromatography. The total procedural blank was 5.4 pg Os and 3.8 pg Re and blank corrections were utilized for all samples. Osmium isotopic compositions were measured on Faraday cups (FC) of the VG Sector 54 instrument. The Os cut of sample 04XG26 was run on both the Faraday cups and secondary electron multiplier of the Sector 54 instrument (Table 3). Additionally, two replicate digestions for sample NSDZ02 were performed to assess the sample powder homogeneity (Table 3). The measured isotopic ratios were corrected for mass fractionation using $^{192}Os/^{188}Os = 3.083$. The $^{187}Os/^{188}Os$ ratio in the Johnson–Matthey Os standard measured during the period of data collection averaged 0.11381 ± 0.00010 ($N=8$, $2\sigma_{S.D.}$) and 0.11378 ± 0.00012 ($N=8$, $2\sigma_{S.D.}$) for the Faraday cups and the electron multiplier, respectively. The measurements of Re were done on a *Nu* Plasma MC-ICP-MS using a triple electron multiplier configuration in static mode. Mass fractionations for Re were corrected using a linear law and $^{185}Re/^{187}Re = 0.5975$ relative to those measured in the Re standard that was run alternately with the samples. To calculate the age, the Re–Os data were regressed using ISOPLOT (Ludwig, 2003). The error input was determined from the external precisions of the standard measurements that were established to be 0.1% for $^{187}Os/^{188}Os$ and 0.5% for $^{187}Re/^{188}Os$. All errors on age and initial isotopic ratio are quoted at $2\sigma_{mean}$.

The accuracy of the analytical techniques applied at the Isotope Geochemistry Laboratory, University of Maryland was assessed by studies of Os isotopic compositions and HSE abundances in the peridotite reference materials UB-N and GP-13 (Puchtel et al., submitted for publication), which are widely used by the HSE community. Concentrations of Re and Os obtained at the University of Maryland agree within analytical uncertainty with those obtained in most other labs (see Table 1 in Puchtel et al., submitted for publication). The average $^{187}Os/^{188}Os$ ratio obtained for the UB-N standard at the University of Maryland agrees well with that reported from Leoben University. Although there are no published $^{187}Os/^{188}Os$ data available to date for the GP-13 standard, an average of multiple analyses obtained at University of Maryland is identical to that obtained at Durham University (0.12647±42: D.G. Pearson, personal communication).

4. Results

4.1. Mineral chemistry

Mineral compositions are given in Table 1. The four samples measured for Re–Os isotopes contain variable amounts of relict primary olivine, clinopyroxene, orthopyroxene and chromite. As described by previous studies (Zhang et al., 2003; Zheng et al., 2005), rounded or ovoid olivine relics are separated by serpentine, show typical mesh texture, and contain ilmenite lamellae. Minor, fine-grained chromite occurs in the matrix or as inclusions in garnet and olivine. Fine-grained (0.03–1.25 mm) garnet occurs as a matrix phase and is partially or completely replaced by very fine-grained aggregates of minerals whose compositions cannot be resolved by probe analysis. Rare, relict garnet occurs in sample 04XG14 (Table 1). The garnet relics are surrounded by brownish kelyphitic rims, whereas rare garnet inclusions in olivine or pyroxene remained unaltered. Diopside is partially replaced by tremolite and orthopyroxene is replaced by fine-grained talc aggregates along crystal margins or microfractures.

Olivines have a high forsterite component ($Fo_{91.0–92.6}$) and extremely low CaO (<0.05%) (Table 1). Chromites have high Cr_2O_3 contents, with Cr# (100×Cr/

Table 1
Compositions of minerals from the Xugou peridotites

Mineral	NSDZ01								NSDZ02								04XG7							
	Chr (n=4)		Cpx (n=3)		Ol (n=8)		Opx (n=2)		Chr (n=4)		Cpx (n=3)		Ol (n=7)		Opx (n=4)		Chr (n=4)		Ol (n=3)		Opx (n=3)		Serp (n=3)	
	Av	σ	Av	σ	Av	σ	Av	σ	Av	σ	Av	σ	Av	σ	Av	σ	Av	σ	Av	σ	Av	σ	Av	σ
SiO_2	0.03	0.01	54.00	0.32	40.70	0.27	57.42	0.21	0.04	0.00	54.79	0.38	40.50	0.24	56.82	0.10	0.00	0.00	41.00	0.21	58.26	0.87	46.68	0.58
TiO_2	0.19	0.10	0.02	0.01	0.01	0.01	0.01	0.00	0.25	0.07	0.03	0.01	0.00	0.00	0.00	0.00	0.40	0.06	0.00	0.00	0.00	0.00	0.00	0.00
Al_2O_3	7.73	1.15	0.48	0.06	0.01	0.01	0.13	0.02	9.16	2.56	1.04	0.07	0.02	0.02	0.14	0.02	14.96	5.64	0.00	0.00	0.22	0.01	0.41	0.13
Cr_2O_3	51.26	1.80	0.64	0.07	0.01	0.02	0.06	0.02	54.21	0.75	1.12	0.04	0.01	0.02	0.05	0.01	41.27	1.39	0.00	0.00	0.01	0.01	0.05	0.04
FeO	32.71	0.98	1.54	0.09	7.40	0.36	5.19	0.02	28.18	2.29	1.89	0.03	7.63	0.66	5.17	0.10	33.85	4.68	8.73	0.21	5.24	0.20	5.92	1.28
MnO	0.78	0.13	0.04	0.02	0.13	0.04	0.00	0.00	0.72	0.10	0.04	0.01	0.17	0.06	0.01	0.01	0.39	0.06	0.06	0.04	0.03	0.03	0.01	0.01
MgO	6.26	0.38	17.49	0.14	51.63	0.26	36.66	0.15	7.28	0.45	16.62	0.22	51.11	0.40	36.44	0.16	7.26	1.66	49.77	0.20	36.25	0.24	33.23	1.64
CaO	0.00	0.00	24.93	0.37	0.01	0.01	0.07	0.02	0.00	0.00	23.56	0.21	0.01	0.01	0.08	0.01	0.00	0.00	0.00	0.00	0.04	0.01	0.23	0.07
Na_2O	0.02	0.02	0.67	0.10	0.02	0.02	0.02	0.00	0.03	0.03	1.39	0.06	0.01	0.01	0.01	0.01	0.00	0.00	0.00	0.00	0.00	0.00	0.00	0.00
K_2O	0.01	0.01	0.02	0.00	0.01	0.01	0.02	0.00	0.00	0.01	0.00	0.00	0.01	0.01	0.00	0.00	0.00	0.00	0.00	0.00	0.00	0.00	0.00	0.00
Total	99.03	0.98	99.86	0.11	100.27	0.52	99.64	0.32	99.92	0.40	100.50	0.73	99.91	0.62	98.79	0.30	98.14	2.43	99.55	0.50	100.05	1.11	86.53	0.92
Mg#	25.45	1.62	95.25	0.29	92.56	0.34	92.61	0.03	31.61	3.05	93.97	0.02	92.28	0.65	92.59	0.11	27.85	7.00	91.05	0.20	92.50	0.21	90.88	2.15
Cr#	81.67	2.55							80.06	4.51							65.87	10.13						
Fo					92.6	0.3							92.3	0.7					91.0	0.2				
En							0.94	0.00							0.94	0.00					0.92	0.00		
Alm																								
Pyr																								
Si	0.00	0.00	1.95	0.01	0.98	0.00	1.97	0.00	0.00	0.00	1.97	0.01	0.98	0.00	1.96	0.00	0.00	0.00	0.99	0.00	1.99	0.01	4.36	0.02
Ti	0.00	0.00	0.00	0.00	0.00	0.00	0.00	0.00	0.01	0.00	0.00	0.00	0.00	0.00	0.00	0.00	0.01	0.00	0.00	0.00	0.00	0.00	0.00	0.00
Al	0.31	0.04	0.02	0.00	0.00	0.00	0.01	0.00	0.36	0.09	0.04	0.00	0.00	0.00	0.01	0.00	0.57	0.20	0.00	0.00	0.01	0.00	0.05	0.01
Cr	1.38	0.04	0.02	0.00	0.00	0.00	0.00	0.00	1.42	0.04	0.03	0.00	0.00	0.00	0.00	0.00	1.08	0.09	0.00	0.00	0.00	0.00	0.00	0.00
Fe^{2+}	1.11	0.04	0.05	0.00	0.18	0.01	0.15	0.00	0.94	0.09	0.06	0.00	0.18	0.02	0.15	0.00	1.13	0.23	0.21	0.00	0.15	0.00	0.55	0.12
Mn	0.02	0.00	0.00	0.00	0.00	0.00	0.00	0.00	0.02	0.00	0.00	0.00	0.00	0.00	0.00	0.00	0.01	0.00	0.00	0.00	0.00	0.00	0.00	0.00
Mg	0.32	0.02	0.94	0.01	1.86	0.01	1.87	0.00	0.36	0.02	0.89	0.01	1.85	0.01	1.88	0.00	0.36	0.06	1.80	0.01	1.85	0.01	4.63	0.19
Ca	0.00	0.00	0.97	0.02	0.00	0.00	0.00	0.00	0.00	0.00	0.91	0.01	0.00	0.00	0.00	0.00	0.00	0.00	0.00	0.00	0.00	0.00	0.02	0.01
Na	0.00	0.00	0.05	0.01	0.00	0.00	0.00	0.00	0.00	0.00	0.10	0.00	0.00	0.00	0.00	0.00	0.00	0.00	0.00	0.00	0.00	0.00	0.00	0.00
K	0.00	0.00	0.00	0.00	0.00	0.00	0.00	0.00	0.00	0.00	0.00	0.00	0.00	0.00	0.00	0.00	0.00	0.00	0.00	0.00	0.00	0.00	0.00	0.00
Total	3.15	0.01	4.10	0.02	3.02	0.00	4.06	0.00	3.10	0.03	4.08	0.01	3.02	0.00	4.07	0.01	3.16	0.06	3.01	0.00	4.01	0.03	9.61	0.03

Sample	04XG11										04XG14											
Mineral	Cpx (n=3)		Grt (n=2)		Ol (n=2)		Opx (n=3)		Serp (n=2)		Chr (n=6)		Cpx (n=2)		Grt (n=2)		Ol (n=7)		Opx (n=2)		Serp (n=2)	
	Av	σ	Av	σ	Av	σ	Av	σ	Av	σ	Av	σ	Av	σ	Av	σ	Av	σ	Av	σ	Av	σ
SiO_2	55.53	0.16	41.98	0.24	41.37	0.17	57.90	0.08	44.23	0.36	0.02	0.02	55.31	0.74	41.55	0.22	40.77	0.46	58.42	0.27	41.99	1.07
TiO_2	0.00	0.00	0.00	0.00	0.00	0.00	0.00	0.00	0.00	0.00	0.20	0.04	0.00	0.00	0.00	0.00	0.01	0.01	0.00	0.00	0.00	0.00
Al_2O_3	0.93	0.05	22.51	0.82	0.00	0.00	0.16	0.02	0.06	0.09	8.01	1.44	0.95	0.00	23.08	0.18	0.00	0.00	0.19	0.03	0.26	0.03
Cr_2O_3	0.85	0.14	1.81	0.31	0.00	0.00	0.00	0.01	0.00	0.00	54.72	1.08	1.20	0.10	2.31	0.93	0.02	0.03	0.00	0.00	0.00	0.00
TFeO	2.13	0.11	10.96	0.16	8.46	0.48	5.22	0.20	1.90	0.14	27.93	1.14	1.69	0.04	9.44	0.66	7.38	0.19	4.59	0.11	4.54	1.57
MnO	0.00	0.00	0.50	0.03	0.02	0.03	0.02	0.02	0.00	0.00	0.63	0.17	0.00	0.00	0.62	0.08	0.08	0.08	0.06	0.00	0.06	0.08
MgO	16.72	0.15	18.51	0.93	49.94	0.08	36.02	0.13	41.41	0.74	7.31	0.44	16.85	0.03	18.91	0.34	51.03	0.29	36.30	0.72	38.70	1.10
CaO	23.06	0.09	3.89	0.49	0.00	0.00	0.04	0.00	0.00	0.00	0.00	0.00	22.30	0.71	4.86	0.40	0.00	0.00	0.04	0.02	0.12	0.03
Na_2O	1.26	0.08	0.00	0.00	0.00	0.00	0.00	0.00	0.00	0.00	0.02	0.03	1.35	0.04	0.00	0.00	0.01	0.02	0.01	0.01	0.00	0.00
K_2O	0.00	0.00	0.00	0.00	0.00	0.00	0.00	0.00	0.00	0.00	0.00	0.00	0.00	0.00	0.00	0.00	0.01	0.01	0.00	0.00	0.00	0.00
Total	100.50	0.38	100.17	0.99	99.79	0.25	99.36	0.34	87.60	1.05	98.86	1.00	99.65	0.05	100.77	0.14	99.63	0.43	99.61	1.16	85.67	0.51

Mg#	93.33	0.36	75.05	1.21	91.32	0.46	92.48	0.24	97.50	0.22	31.82	1.62	94.67	0.14	78.15	0.88	92.50	0.19	93.38	0.02	93.83	2.17
Cr#											82.16	2.58										
Fo					91.3	0.5											92.5	0.2				
En							0.92	0.00											0.93	0.00		
Alm			22.17	0.70											18.87	1.00						
Pyr			66.72	2.22											67.42	0.10						
Si	2.00	0.01	3.01	0.02	1.00	0.00	1.99	0.01	4.07	0.02	0.00	0.00	2.00	0.03	2.96	0.01	0.99	0.01	2.00	0.02	4.00	0.04
Ti	0.00	0.00	0.00	0.00	0.00	0.00	0.00	0.00	0.00	0.00	0.01	0.00	0.00	0.00	0.00	0.00	0.00	0.00	0.00	0.00	0.00	0.00
Al	0.04	0.00	1.90	0.04	0.00	0.00	0.01	0.00	0.01	0.01	0.32	0.05	0.04	0.00	1.94	0.01	0.00	0.00	0.01	0.00	0.03	0.00
Cr	0.02	0.00	0.10	0.02	0.00	0.00	0.00	0.00	0.00	0.00	1.46	0.02	0.03	0.00	0.13	0.05	0.00	0.00	0.00	0.00	0.00	0.00
Fe^{2+}	0.06	0.00	0.66	0.02	0.20	0.01	0.15	0.01	0.17	0.01	0.94	0.05	0.05	0.00	0.56	0.04	0.18	0.00	0.13	0.00	0.43	0.16
Mn	0.00	0.00	0.03	0.00	0.00	0.00	0.00	0.00	0.00	0.00	0.02	0.00	0.00	0.00	0.04	0.00	0.00	0.00	0.00	0.00	0.00	0.01
Mg	0.90	0.00	1.98	0.07	1.80	0.00	1.85	0.00	5.68	0.03	0.37	0.02	0.91	0.00	2.01	0.03	1.84	0.01	1.85	0.01	5.50	0.08
Ca	0.89	0.01	0.30	0.04	0.00	0.00	0.00	0.00	0.00	0.00	0.00	0.00	0.87	0.03	0.37	0.03	0.00	0.00	0.00	0.00	0.01	0.00
Na	0.09	0.01	0.00	0.00	0.00	0.00	0.00	0.00	0.00	0.00	0.00	0.00	0.09	0.00	0.00	0.00	0.00	0.00	0.00	0.00	0.00	0.00
K	0.00	0.00	0.00	0.00	0.00	0.00	0.00	0.00	0.00	0.00	0.00	0.00	0.00	0.00	0.00	0.00	0.00	0.00	0.00	0.00	0.00	0.00
Total	4.03	0.01	7.98	0.01	3.00	0.00	4.01	0.01	9.93	0.01	3.11	0.02	4.01	0.05	8.01	0.01	3.01	0.01	3.99	0.03	9.98	0.04

Sample	04XG15								04XG26									04XG38						
Mineral	Cpx	Grt (n=2)		Ol (n=2)		Opx (n=2)		Serp	Chr (n=4)		Ol (n=6)		Opx (n=4)		Phl	Serp (n=3)		Chr	Cpx	Grt (n=2)		Ol	Opx	Serp
		Av	σ	Av	σ	Av	σ		Av	σ	Av	σ	Av	σ		Av	σ			Av	σ			
SiO_2	55.40	42.09	0.56	41.62	42.43	58.20	0.52	42.43	0.03	0.03	40.70	0.42	58.73	0.27	41.82	43.20	0.53	0.00	55.61	42.37	0.41	41.61	58.68	43.42
TiO_2	0.00	0.00	0.00	0.00	0.00	0.00	0.00	0.00	0.16	0.08	0.00	0.00	0.00	0.00	0.18	0.00	0.00	0.03	0.00	0.00	0.00	0.00	0.00	0.00
Al_2O_3	1.91	22.90	0.38	0.00	0.36	0.16	0.02	0.36	10.34	2.53	0.00	0.00	0.17	0.02	14.80	0.00	0.00	23.25	1.61	23.19	0.20	0.00	0.14	0.33
Cr_2O_3	1.53	1.33	0.17	0.00	0.00	0.00	0.00	0.00	51.76	1.90	0.00	0.00	0.00	0.00	0.62	0.01	0.02	36.57	0.84	1.39	0.33	0.00	0.00	0.00
FeO	3.68	10.86	0.22	9.00	4.13	4.87	0.35	4.13	28.78	1.48	7.88	0.24	4.68	0.08	2.44	3.25	0.39	24.29	2.71	10.73	0.74	8.43	5.14	2.94
MnO	0.00	0.50	0.03	0.08	0.00	0.03	0.03	0.00	0.69	0.06	0.10	0.03	0.05	0.03	0.00	0.02	0.02	0.18	0.00	0.63	0.05	0.04	0.09	0.01
MgO	15.33	18.72	0.33	50.08	39.96	36.19	0.42	39.96	7.11	0.73	50.87	0.36	36.89	0.44	24.78	39.90	0.56	10.41	15.62	18.87	0.12	50.52	36.39	41.13
CaO	20.55	4.24	0.34	0.00	0.00	0.11	0.09	0.00	0.00	0.01	0.00	0.01	0.02	0.02	0.00	0.04	0.03	0.00	21.64	3.85	0.50	0.00	0.10	0.00
Na_2O	2.35	0.00	0.00	0.00	0.00	0.00	0.00	0.00	0.03	0.01	0.00	0.01	0.00	0.00	1.14	0.00	0.00	0.00	2.02	0.00	0.00	0.00	0.00	0.00
K_2O	0.00	0.00	0.00	0.00	0.00	0.00	0.00	0.00	0.01	0.01	0.00	0.00	0.00	0.00	6.80	0.00	0.00	0.00	0.00	0.00	0.00	0.00	0.00	0.00
Total	100.74	100.65	0.92	100.78	86.89	99.56	1.25	86.89	98.98	0.39	99.82	0.42	100.53	0.70	92.58	86.42	0.51	94.72	100.03	101.03	0.20	100.61	100.54	87.82
Mg#	88.14	75.45	0.70	90.85	94.52	92.98	0.39	94.52	30.60	3.21	92.01	0.27	93.36	0.15	94.76	95.63	0.44	43.30	91.14	75.82	1.37	91.44	92.66	96.15
Cr#									77.18	5.05								51.35						
Fo				90.8							92.0	0.3										91.5		
En						0.93	0.00						0.93	0.00									0.93	
Alm		21.65	0.42																	21.50	1.54			
Pyr		66.52	1.22																	67.35	0.21			
Si	1.99	3.00	0.00	1.00	3.98	2.00	0.01	3.98	0.00	0.00	0.99	0.00	1.99	0.01	2.96	4.05	0.05	0.00	2.01	3.01	0.01	1.00	2.00	4.01
Ti	0.00	0.00	0.00	0.00	0.00	0.00	0.00	0.00	0.00	0.00	0.00	0.00	0.00	0.00	0.01	0.00	0.00	0.00	0.00	0.00	0.00	0.00	0.00	0.00
Al	0.08	1.93	0.01	0.00	0.04	0.01	0.00	0.04	0.41	0.09	0.00	0.00	0.01	0.00	1.23	0.00	0.00	0.88	0.07	1.94	0.01	0.00	0.01	0.04
Cr	0.04	0.07	0.01	0.00	0.00	0.00	0.00	0.00	1.37	0.07	0.00	0.00	0.00	0.00	0.03	0.00	0.00	0.93	0.02	0.08	0.02	0.00	0.00	0.00
Fe^{2+}	0.11	0.65	0.02	0.22	0.39	0.14	0.01	0.39	0.96	0.07	0.19	0.01	0.13	0.00	0.17	0.31	0.04	0.78	0.08	0.64	0.05	0.20	0.15	0.27
Mn	0.00	0.03	0.00	0.00	0.00	0.00	0.00	0.00	0.02	0.00	0.00	0.00	0.00	0.00	0.00	0.00	0.00	0.00	0.00	0.04	0.00	0.00	0.00	0.00
Mg	0.82	1.99	0.01	1.79	5.59	1.85	0.00	5.59	0.35	0.03	1.84	0.01	1.87	0.01	2.61	5.58	0.07	0.50	0.84	2.00	0.00	1.80	1.85	5.66
Ca	0.79	0.32	0.03	0.00	0.00	0.00	0.00	0.00	0.00	0.00	0.00	0.00	0.00	0.00	0.00	0.00	0.00	0.00	0.84	0.29	0.04	0.00	0.00	0.00
Na	0.16	0.00	0.00	0.00	0.00	0.00	0.00	0.00	0.00	0.00	0.00	0.00	0.00	0.00	0.16	0.00	0.00	0.00	0.14	0.00	0.00	0.00	0.00	0.00
K	0.00	0.00	0.00	0.00	0.00	0.00	0.00	0.00	0.00	0.00	0.00	0.00	0.00	0.00	0.61	0.00	0.00	0.00	0.00	0.00	0.00	0.00	0.00	0.00
Total	4.06	8.00	0.01	3.00	10.00	4.00	0.01	10.00	3.11	0.01	3.01	0.01	4.01	0.02	7.79	9.95	0.06	3.09	4.03	7.99	0.01	3.00	4.00	9.97

Av, average; σ, standard deviation; Alm, almandine; Chr, chromite; Cpx, clinopyroxene; Fo, forsterite; Grt, garnet; Ol, olivine; Opx, orthopyroxene; Phl, phlogopite; Pyr, pyrope; Serp, serpentine; Cr#=100×Cr/(Cr+Al); Mg#=100×molar Mg/(Mg+Fe).

Table 2
Chemical compositions of Xugou peridotites

	SiO_2	TiO_2	Al_2O_3	TFe_2O_3	MnO	MgO	NiO	CaO	Na_2O	K_2O	P_2O_5	H_2O	CO_2	LOI	Sum	Mg#
NSDZ01	38.04	0.01	0.38	7.40	0.09	41.92	0.27	0.26	0.01	0.03	0.01			12.23	100.37	91.8
NSDZ02	38.78	0.01	0.96	7.18	0.09	40.28	0.29	0.51	0.05	0.1	0.01			12.06	100.03	91.8
NSDZ03	40.34	0.01	1.22	7.30	0.09	40.16	0.25	0.84	0.08	0.01	0.01			10.12	100.17	91.6
NSDZ04	40.08	0.05	1.89	8.03	0.11	38.08	0.25	1.39	0.11	0.02	0.01			9.94	99.71	90.4
NSDZ05	38.52	0.01	1.07	7.25	0.10	38.87	0.28	0.25	0.06	0.02	0.01			13.64	99.80	91.4
04XG7	41.62	0.09	1.70	7.94	0.12	34.69	0.24	0.96	0.04	0.01	0.01	11.99	0.45		99.86	89.6
04XG11	44.53	0.12	3.44	10.07	0.11	30.95	0.26	2.04	0.11	0.01	0.01	8.18	0.17		100.00	85.9
04XG14	40.87	0.04	0.20	7.37	0.11	39.44	0.25	0.27	0.01	0.02	0.01	11.32	0.20		100.11	91.4
04XG15	42.26	0.12	2.76	8.74	0.13	32.17	0.22	2.35	0.09	0.01	0.01	10.13	1.02		100.01	87.9
04XG26	42.18	0.04	0.92	7.94	0.11	38.17	0.24	0.88	0.08	0.08	0.03	9.14	0.33		100.15	90.5
04XG38	42.68	0.11	2.72	8.71	0.13	33.02	0.22	1.46	0.17	0.01	0.01	10.73	0.10		100.06	88.3
Recal*																
NSDZ01	43.02	0.01	0.43	8.37	0.10	47.41	0.31	0.29	0.01	0.03	0.01				100.00	
NSDZ02	43.94	0.01	1.09	8.14	0.10	45.64	0.33	0.58	0.06	0.11	0.01				100.00	
NSDZ03	44.67	0.01	1.35	8.08	0.10	44.47	0.28	0.93	0.09	0.01	0.01				100.00	
NSDZ04	44.52	0.06	2.10	8.92	0.12	42.30	0.28	1.54	0.12	0.02	0.01				100.00	
NSDZ05	44.56	0.01	1.24	8.39	0.12	44.97	0.32	0.29	0.07	0.02	0.01				100.00	
04XG7	47.61	0.10	1.94	9.08	0.14	39.68	0.27	1.10	0.05	0.01	0.01				100.00	
04XG11	48.59	0.13	3.75	10.99	0.12	33.77	0.28	2.23	0.12	0.01	0.01				100.00	
04XG14	46.13	0.05	0.23	8.31	0.12	44.52	0.29	0.30	0.01	0.02	0.01				100.00	
04XG15	47.56	0.14	3.11	9.84	0.15	36.20	0.24	2.64	0.10	0.01	0.01				100.00	
04XG26	46.52	0.04	1.01	8.76	0.12	42.10	0.27	0.97	0.09	0.09	0.03				100.00	
04XG38	47.83	0.12	3.05	9.76	0.15	37.00	0.24	1.64	0.19	0.01	0.01				100.00	

	NSDZ01	NSDZ02	NSDZ03	NSDZ04	NSDZ05	04XG7	04XG11	04XG14	04XG15	04XG26	04XG38
Li	1.5	1.4		2.4	2.3	2.4	6.9	1.0	7.4	0.6	7.4
Be	0.024	0.041	0.006	0.010	0.002	0.079	0.097	0.007	0.093	0.007	0.072
Sc	5.8	7.6	6.6	13	9.6	8.0	17	3.2	49	4.6	9.8
V	21	36	34	58	36	41	77	14	67	15	73
Cr	3220	3260	2380	2839	2845	986	3546	2470	3530	2350	3491
Co	98	102	91	109	110	89	189	97	123	94	120
Cu	5.1	6.4		11	11	10	24	6.1	31	2.3	25
Zn	44	46	26	46	44	34	51	37	48	37	52
Ga	0.42	0.71	0.85	2.0	1.0	1.2	3.1	0.34	2.8	0.26	2.8
Rb	0.84	4.8	0.87	0.63	1.0	0.28	0.31	0.79	0.25	0.31	0.47
Sr	9.9	26	9.2	10	6.8	9.5	25	6.6	29	12	15
Y	0.68	0.39	0.19	1.4	0.26	1.2	7.5	0.17	3.0	0.15	2.7
Zr	0.16	0.34	0.50	0.85	0.26	1.2	4.0	0.10	3.8	0.32	1.8
Nb	1.1	0.26	0.07	0.19	0.20	0.07	0.06	0.08	0.05	0.07	0.03
Ba	32	121	10	13	22	15	23	46	41	18	57
La	5.4	0.44	0.10	0.29	0.27	0.23	3.3	0.12	0.37	0.10	0.31
Ce	7.9	0.83		0.59	0.45	0.55	5.2	0.32	0.71	0.25	0.60
Pr	0.60	0.089	0.015	0.077	0.049	0.054	0.81	0.052	0.11	0.037	0.10
Nd	1.5	0.34	0.049	0.33	0.16	0.30	3.7	0.3	0.6	0.2	0.5
Sm	0.11	0.040	0.017	0.092	0.024	0.094	0.80	0.032	0.20	0.017	0.20
Eu	0.027	0.013	0.006	0.037	0.007	0.032	0.28	0.010	0.086	0.006	0.091
Gd	0.084	0.041	0.018	0.12	0.023	0.11	0.93	0.026	0.32	0.017	0.29
Tb	0.014	0.0065	0.0030	0.024	0.0041	0.020	0.17	0.0034	0.065	0.0027	0.06
Dy	0.077	0.041	0.020	0.19	0.026	0.16	1.0	0.019	0.44	0.013	0.41
Ho	0.016	0.009	0.006	0.047	0.006	0.035	0.23	0.003	0.11	0.002	0.10
Er	0.049	0.027	0.021	0.14	0.023	0.11	0.61	0.009	0.30	0.005	0.28
Tm	0.008	0.005	0.004	0.021	0.004	0.015	0.10	0.0015	0.051	0.001	0.046
Yb	0.055	0.040	0.036	0.17	0.035	0.10	0.60	0.010	0.35	0.004	0.32
Lu	0.008	0.007	0.008	0.025	0.007	0.016	0.10	0.001	0.055	0.0006	0.052
Ta	0.073	0.088		0.074	0.065	0.011	0.0059	0.087	0.0033	0.066	0.0029
Pb	1.2	2.3	1.9	0.71	2.7	3.0	10	0.65	2.2	1.2	3.9
Th	0.56	0.53		0.005		0.021	0.011	0.11		0.008	
U	0.057	0.16		0.004	0.008	0.44	0.76	0.24	0.56	0.013	0.065

*Recalculated to 100% anhydrous.
Major elements are reported in wt.% and trace elements in ppm.

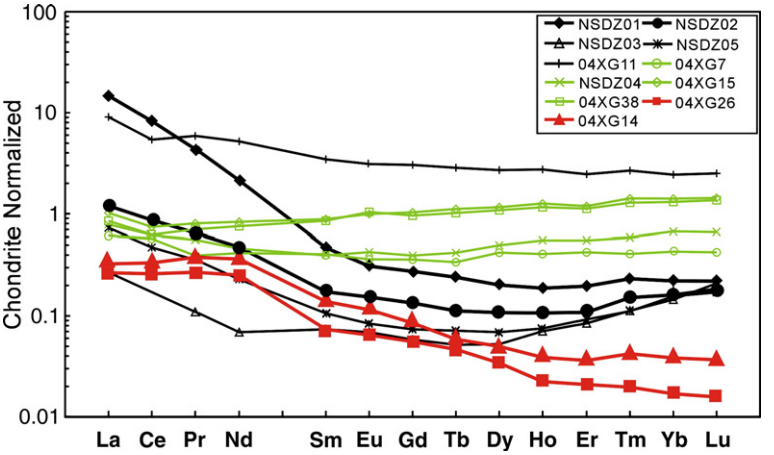

Fig. 3. Chondrite-normalized rare earth element patterns of Xugou peridotites. Chondrite values are from Taylor and McLennan (1985).

(Cr+Al))=51–82 and low Mg# (100×molar Mg/(Mg+Fe)=23–35), compositions that are similar to inclusions in diamond and to chromite in cratonic xenoliths and alpine type peridotites (Zhang et al., 2003). These olivine and chromite compositions reflect the very refractory compositions of these samples (Zhang et al., 2003; Zheng et al., 2005, 2006c). Orthopyroxene (En_{92-93}) has low Al_2O_3 content (0.13–0.22%); garnet is characteristically Cr-bearing (1.3–2.3%) and pyrope-rich. These features imply a pressure of ~5 GPa for estimated temperatures of 780–870 °C (Zhang et al., 2005).

4.2. Major and trace element geochemistry

Major and trace element compositions of the Xugou peridotites are listed in Table 2. All samples contain very high LOI (Loss on Ignition) and H_2O content since they are serpentinized to different extents. Accordingly, we normalized the major element concentrations to 100% anhydrous, in order to compare with data reported elsewhere. The Xugou peridotites have variable whole-rock compositions: Al_2O_3 (0.23–3.75%), total Fe_2O_3 (8.08–10.99%), CaO (0.29–2.64%) MgO (33.8–47.4%) and

Table 3
Re–Os isotopic compositions of mantle peridotites from Sulu and Dabie terranes

	Re	Os	$^{187}Re/^{188}Os$	$^{187}Os/^{188}Os$	2σ	T_{RD}	T_{MA}	Mg#	Fo	Cr#	$Al_2O_3^*$	MgO*
	(ppb)	(ppb)				(Ga)	(Ga)	(W.R.)		Chromite	(wt.%)	(wt.%)
Xugou, Sulu (this study)												
NSDZ01(FC)	0.055	4.47	0.059	0.11672	11	1.8	2.0	91.8	92.6	81.7	0.43	47.4
NSDZ02(FC)	0.042	3.28	0.062	0.11639	19	1.8	2.1	91.8	92.3	80.1	1.09	45.6
NSDZ02 duplicate(FC)	0.049	3.45	0.068	0.11604	8	1.8	2.2					
04XG14(FC)	0.044	2.99	0.071	0.11773	12	1.6	1.9	91.4	92.5	82.2	0.23	44.5
04XG26 (FC)	0.045	6.15	0.035	0.11582	19	1.9	2.0	90.5	92.0	77.2	1.01	42.1
04XG26 (EM)	0.045	6.18	0.035	0.11484	27	2.0	2.2					
Raobazhai, Dabie (Jin et al., 2004)												
ZK4-13U	0.232	3.76	0.297	0.11972	7	1.4	4.2				2.09	40.0
ZK4-56L	0.370	0.69	2.564	0.12539	43	0.6	Future				2.94	36.8
ZK84-10U	0.335	3.27	0.493	0.12308	28	0.9	Future				3.37	36.8
ZK84-48L	0.010	0.76	0.061	0.11652	61	1.8	2.1				1.23	41.1
ZK84-58L	0.004	0.93	0.022	0.11853	73	1.5	1.6				0.82	43.1
ZK84-69L	0.007	0.89	0.040	0.11963	95	1.4	1.5				0.99	41.8
ZK90-5U	0.249	3.19	0.375	0.13061	13	Future	Future				3.60	34.5
ZK90-7U	0.182	2.58	0.339	0.11739	7	1.7	7.33				0.85	42.6
ZK92-12U	0.098	3.35	0.276	0.12064	16	1.2	3.3				1.97	38.8

*Normalized to 100% volatile-free. Two replicate digestions for sample NSDZ02 were performed at different analytical sessions while the same Os cut of sample 04XG26 was run on both FC and EM. FC, Faraday cups. EM, secondary Electron Multiplier. All the reported values were corrected for mass fractionation and blank (Os=5.4 pg, and Re=3.8 pg). Primitive upper mantle (PUM) values are taken from Meisel et al. (2001) and Bennett et al. (2002) ($^{187}Os/^{188}Os = 0.1296\pm8$, $^{187}Re/^{188}Os = 0.435\pm5$). The λ_{Re} used in the calculation is 1.666×10^{-11}/year (Morgan, 1985).

Mg# (85.9–91.8%), and show negative correlations between whole-rock MgO and TiO_2, Al_2O_3, total Fe_2O_3 and CaO (correlation coefficient $r=-0.90$ to -0.95) and positive correlations between whole-rock Al_2O_3 and CaO and some incompatible elements (Li, V, Cu, Ga, Sr, Y, Zr, HREEs, Hf, Pb and U) ($r=0.69$ to 0.98) (Fig. 2). The trends are similar to those of peridotite xenoliths from Hannuoba, Qixia and Longgang of the NCC (Gao et al., 2002; Wu et al., 2003; Rudnick et al., 2004) and from the Subei basin (Reisberg et al., 2005) and peridotites from the Dabie terrane (Jin et al., 2004), which are interpreted to reflect melt depletion. The Xugou peridotites with MgO > 40% (including the four samples measured for Re–Os isotopes) fall on the trends defined by the other peridotites. However those with MgO < 40% plot off the trend at lower CaO and Al_2O_3 for a given MgO, which we attribute to serpentinization. The four samples investigated for Re–Os isotopic analyses were selected as being the most refractory among the Xugou peridotite suite. This is also supported by the significantly higher average forsterite components of their olivines ($Fo_{92.0–92.6}$) compared to those of other samples ($Fo_{90.8–91.5}$). Samples NSDZ01 and NSDZ02 have a higher Mg/Si than the other two samples, consistent with a higher proportion of olivine to orthopyroxene.

The four samples selected for Os isotope analyses exhibit light rare earth element (LREE) enriched patterns, like the most of the peridotites from Xugou (Fig. 3). Generally, there are three types of whole rock REE patterns: 1) 04XG11, NSDZ01 and NSDZ02 are LREE enriched and show higher REE concentrations than NSDZ03 and NSDZ05. NSDZ01 has the highest LREE abundances of all samples studied here. 2) 04XG14 and 04XG26 show similar REE patterns but with relatively flat LREE distribution. 3) The remaining samples, including 04XG15, 04XG7, 04XG38 and NSDZ04, have a relatively flat REE distribution, with chondrite normalized values close to one.

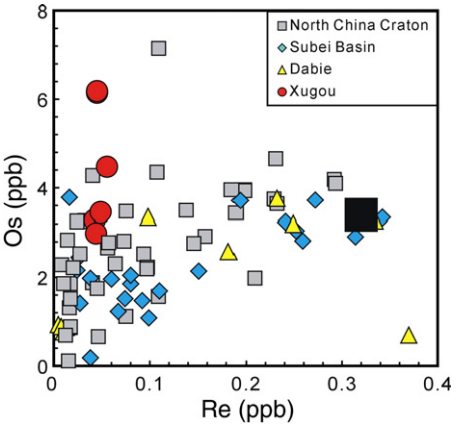

Fig. 4. Re versus Os concentrations of Xugou peridotites (circles) compared to mantle peridotites from the Dabie terrane (triangles) (Jin et al., 2004) and peridotite xenoliths from Hannuoba and Qixia (Rudnick et al., 2004) and Longgang and Kuandian (Wu et al., 2003, 2006) of the North China craton (squares) and from the Subei basin (diamonds) (Reisberg et al., 2005).

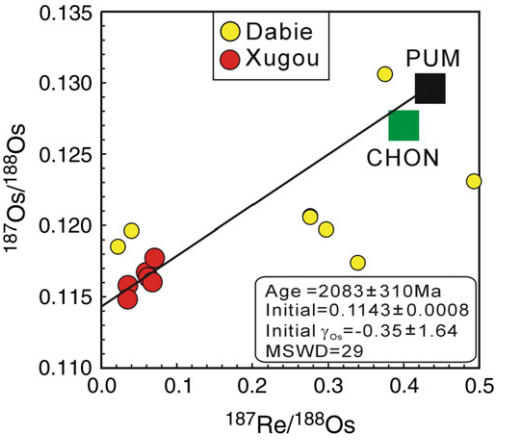

Fig. 5. Re–Os isochron diagrams for Xugou peridotites. Also shown are data for mantle peridotites from the Dabie terrane (Jin et al., 2004). PUM (primitive upper mantle) values from Meisel et al. (2001); CHON represents the chondritic reference (Shirey and Walker, 1998). The isochron is forced through estimates of present-day PUM. Data were regressed and MSWD were determined using ISOPLOT (Ludwig, 2003).

4.3. Re–Os systematics

Re–Os isotopic data for the Xugou peridotites are listed in Table 3. Osmium contents of the four samples vary by a factor of 2, from 3.0 to 6.2 ppb, at relatively constant Re contents of 0.045–0.055 ppb (Fig. 4). The Os concentrations are typical of mantle peridotites, while the Re concentrations are lower than the estimated upper mantle average of about 0.26 ppb (Morgan, 1985). The $^{187}Re/^{188}Os$ ratios vary from 0.035 to 0.071 and are all subchondritic (Fig. 5), consistent with a prior melt depletion history. The $^{187}Re/^{188}Os$ isotopic ratios show a broadly positive correlation with $^{187}Os/^{186}Os$ ($r=0.79$).

5. Discussion

5.1. Effects of serpentinization and metasomatism

The Xugou peridotites are heavily serpentinized and some of them contain phlogopite (e.g., 04XG26) and zircon, indicative of metasomatism (Zheng et al., 2005, 2006a,c). Based upon zircon U–Pb ages and Hf isotopic compositions, the metasomatism may be multi-phased

(e.g., Triassic, Mesoproterozoic, Zheng et al., 2006a,b). Thus, the effects of serpentinization and/or metasomatism on Re–Os isotopic systematics must be evaluated before they can be used to infer the age and origin of these mantle peridotites.

The correlations illustrated in Fig. 2 suggest that the whole-rock chemical characteristics are primarily controlled by a single melt extraction event, and that later serpentinization and metasomatism did not obliterate these primary characteristics, even for highly incompatible and soluble to moderately soluble elements such as Ca, V, and U (Rudnick and Gao, 2003).

However, the LREE enrichments observed for whole-rocks from this study (Fig. 3) and for clinopyroxene (Zheng et al., 2005) imply their addition subsequent to melt extraction. Such enriched REE patterns are typical of refractory peridotite xenoliths world-wide (McDonough and Frey, 1989). Addition of LREE may have been accompanied by addition of Re as well, as suggested by sample NSDZ01, which contains the highest Re, REE and Th contents (Table 1). However, there are no correlations between $^{187}Re/^{188}Os$ or $^{187}Os/^{188}Os$ with either La or Re (r=0.00 to 0.17), suggesting that, if it occurred, Re addition was fairly recent (<500 Ma), so that it did not affect the Os isotopic composition through radiogenic in-growth. Moreover, the variation in $^{187}Re/^{188}Os$ ratios within these samples reflects primarily the factor of two variation in Os concentrations at relatively constant and low Re concentrations (0.044 to 0.055 ppb) (Fig. 4). Such low concentrations are inconsistent with sulfide metasomatism. Collectively, these observations suggest that the correlation between $^{187}Os/^{188}Os$ and $^{187}Re/^{188}Os$ ratios (Fig. 5) most likely reflect an ancient melting event.

5.2. Age and origin of Sulu mantle peridotite

Zircon U–Pb dating of eclogites and surrounding gneisses from the Dabie–Sulu UHP belt, together with studies of mineral inclusions in zircon and oxygen isotopes reveal that:

(1) The protoliths of the eclogites and gneisses derive from the Yangtze basement on the basis of Neoproterozoic ages of inherited zircons (650–820 Ma, Ames et al., 1996; Hacker et al., 1998; Ayers et al., 2002; Zheng et al., 2003 and references therein).
(2) Continental crust, represented by the eclogites and gneisses, was subducted to great depth (>180–200 km) and experienced UHP metamorphism during the Triassic subduction of the Yangtze craton beneath the NCC (Ye et al., 2000a,b; Liu et al., 2004).
(3) Subduction and exhumation of UHP rocks was rapid, since the extremely light oxygen isotopic compositions ($\delta^{18}O$ values are as low as −11%) derived from meteoric-hydrothermal alteration prior to the UHP metamorphism are preserved (Zheng et al., 2003, and references therein).

However, where exactly the peridotites fit into this picture is unclear. As stated previously, they could represent 1) Precambrian continental lithospheric mantle from the Yangtze craton, 2) Archean continental lithospheric mantle from the NCC, 3) Triassic mantle wedge peridotite. Since lithospheric mantle forms as a result of melt extraction, determining the melt extraction age of these peridotites could help to distinguish which of these hypotheses is correct.

There are several ways that Re–Os isotopes can be used to obtain a melt depletion age of peridotites (Walker et al., 1989; Reisberg and Lorand, 1995; Handler et al., 1997; Shirey and Walker, 1998; Pearson, 1999; Gao et al., 2002; Wu et al., 2003; Carlson et al., 2005), including: (1) an Re–Os isochron, which is rarely obtained for a number of reasons (e.g., lack of spread in Re/Os, Re mobility, presence of multiple melting events); (2) Using the intercept of correlations between $^{187}Os/^{188}Os$ and an immobile element that exhibits a similar degree of incompatibility as Re during mantle melting (e.g., Al_2O_3, CaO, HREE and Y) and comparing the intercept Os isotopic ratio to a model mantle evolution trend; (3) Calculating an Re–Os model age, T_{MA}, which is determined by using the observed Re/Os ratio and calculating when the sample had a $^{187}Os/^{188}Os$ matching primitive upper mantle. However, like the isochron method, this type of model age relies on Re immobility, which is often a problem for mantle xenoliths; (4) Calculating an Re-depletion model age, T_{RD}, which simply compares the $^{187}Os/^{188}Os$ (corrected to eruption age, in the case of xenoliths), to a mantle evolution model, with the assumption that no Re is retained in the residue after partial melting. Accordingly, T_{RD} ages provide a minimum estimate of the timing of melt depletion, but are good approximations of the time of melting for highly refractory peridotites.

As discussed above, the Re content and Re/Os isotopic ratios of the Xugou peridotites are significantly below primitive mantle values and $^{187}Os/^{188}Os$ correlates with $^{187}Re/^{188}Os$, consistent with variable Re loss via melt depletion and inconsistent with significant exchange during serpentinization and/or metasomatism. As the four samples are the most refractory among the Xugou peridotite suite, they show limited variations in whole-rock and mineral chemistry and, therefore, it is

not possible to obtain reliable $^{187}Os/^{188}Os$ intercept ratios. The T_{RD} ages of the four Xugou peridotites range from 1600 to 2000 Ma, and the T_{MA} ages from 1900 to 2200 Ma. If forced through the primitive upper mantle value (PUM of Meisel et al., 2001), the Xugou peridotites yield an errorchron age of 2083±310 Ma (2σ) (Fig. 5) with MSWD=29 and initial $^{187}Os/^{188}Os$=0.1143± 0.0008 (2σ), corresponding to an initial γ_{Os}=−0.35± 1.64. Since the T_{RD} age provides a minimum estimate of the timing of melt depletion, the maximum T_{RD} age of a suite of mantle peridotites formed via a single event of melt extraction provides the best age constraint on the melting event. Accordingly, the maximum T_{RD}, the average T_{MA} and the errorchron ages return the same value of ~2.0 Ga. Therefore, 2 Ga is our preferred age for formation of the Sulu peridotites.

Jin et al. (2004) analyzed the chemical and Re–Os isotopic compositions of nine serpentinized harzburgites from the Raobozhai mafic–ultramafic body from the Dabie terrane (Fig. 1). Like Xugou, this body is in fault contact with felsic gneisses and is dominated by harzburgite with minor dunite, lherzolite, eclogite and garnet pyroxenite. Major and trace elements compositions of the Raobozhai peridotites also exhibit melt depletion trends (Zhi et al., 2004; Fig. 2), and their olivines have $Fo_{92–93}$ and orthopyroxene $En_{92–93}$ (Wang et al., 2005). Unlike the Xugou peridotites, T_{RD} (−140 to 1790 Ma) and T_{MA} ages (−6900 to 7330 Ma) of the Raobozhai peridotites vary widely from geologically meaningless to future ages. These indicate that the Re–Os isotopic system was disturbed. Samples with Al_2O_3<2.1% have $T_{RD}\geq$ 1.4 Ga, whereas the younger and future T_{RD} ages are confined to the samples with Al_2O_3>2.1% (Table 3). On the other hand, all of the Raobozhai samples show strong correlations of $^{187}Os/^{188}Os$ ratios with Yb (r=0.93) and Al_2O_3 (r=0.89), which suggests that the disturbance resulted from recent mobility of Re, while Os remained immobile. The intercepts of these correlations yield initial $^{187}Os/^{188}Os$ ratios between 0.1141 and 0.1164 (Jin et al., 2004), which correspond to T_{RD} ages of 1800–2100 Ma. These ages are indistinguishable from that obtained from the initial $^{187}Os/^{188}Os$ and are also within the measured range of model ages for the Xugou peridotites. We thus conclude that the Sulu and Dabie peridotites derived from the same source.

Zheng et al. (2006a,c) show that, like the Xugou peridotites, garnet peridotites from the CCSD pre-pilot hole are also refractory (with olivine $Fo_{90.6–92.4}$) and are metasomatized. Based on the refractory compositions and relatively unradiogenic Hf isotopic compositions of zircons (yielding Proterozoic model ages), they suggest that these garnet peridotites derive from refractory Archean mantle that experienced Mesoproterozoic metasomatism (1.2 to 1.4 Ga) and represent a tectonic intrusion into younger crust. However, their data do not negate the possibility that the Sulu peridotites represent fragments of subducted Yangtze CLM.

Knowing the CLM age of the North China and Yangtze cratons *prior to the Triassic* (when the two cratons collided to form the Dabie–Sulu UHP belt and exhumed its mantle peridotites) is key to understanding the derivation of the Dabie–Sulu peridotites. The Sulu terrain is bounded by the eastern block of the NCC in the north and west and by the Yangtze craton in the south (Fig. 1). Various lines of evidence suggest that the eastern block of the NCC has lost its lithospheric keel during the Late Mesozoic, perhaps extending into the Cenozoic (e.g., Menzies et al., 1993; Griffin et al., 1998; Xu, 2001; Gao et al., 2002; Wu et al., 2003; Gao et al., 2004; Wu et al., 2006; Zhang et al., 2006). Three Ordovician kimberlites that carry peridotite xenoliths, occur in the northern (Tieling), central (Fuxian) and southern (Mengyin) parts of the eastern block of the NCC (Fig. 1). Of these, the Fuxian and Mengyin kimberlites are diamond-bearing. Gao et al. (2002) first reported Archean T_{RD} ages (2.5–2.8 Ga) for two peridotite xenoliths from the Fuxian kimberlite and a Proterozoic age for a peridotite from Mengyin, but the latter had anomalously high Re and Re/Os. These data have been significantly augmented by two recent studies. Wu et al. (2006) analyzed seven peridotite xenoliths from the Tieling kimberlite. The most refractory samples have T_{RD} and T_{MA} ages of 2.3–2.5 Ga. They also analyzed four xenocrystic chromite separates (two from Fuxian and one each from Tieling and Mengyin), which yield T_{RD} and T_{MA} ages of 2.7–3.7 Ga. Zhang et al. (2006; Zhang, personal comm.) reported Archean T_{RD} ages (2.5–2.7 Ga) for three peridotite xenoliths from the Mengyin kimberlite and slightly older ages (2.6–3.2 Ga) for seven peridotite xenoliths from the Fuxian kimberlite. Thus, the Archean age of the CLM of the eastern block of the NCC prior to the time of the kimberlite eruption is well established. Because no significant thermo-magmatic activities occurred in the NCC during the Paleozoic, we suggest that the Archean CLM persisted beneath the eastern block until the Triassic collision between the North China and Yangtze cratons. This Archean CLM was replaced during the Mesozoic to Cenozoic by more fertile lithospheric mantle whose Re–Os isotopic compositions (as shown by peridotite xenoliths from Cenozoic basalts at Qixia, Longgang and Kuandian; Fig. 1) are similar to those of modern convecting mantle (Gao et al., 2002; Wu et al., 2003, 2006). This interpretation is also supported by the presence of

extensive magmatism throughout eastern China during the Jurassic and Cretaceous, including the North China and Yangtze cratons (Wu et al., 2005).

Studies of the Hannuoba peridotite xenoliths carried in Cenozoic basalt suggest that the original Archean CLM beneath the Trans-North China Orogen of the NCC (Fig. 1) was removed and replaced around 1.9 Ga ago and the newly formed Paleoproterozoic mantle persists to the present time (Gao et al., 2002; Rudnick et al., 2004). Although similar Paleoproterozoic Os model ages are observed in a few mantle xenoliths carried in Cenozoic basalts that erupted through the Paleoproterozoic orogenic belt along the northern margin of the eastern block of the NCC at Longgang and Kuandian (Fig. 1; Wu et al., 2003, 2006), the majority of xenoliths at these two localities and at Qixia (Fig. 1; Gao et al., 2002) have Re–Os isotopic compositions similar to those of modern convecting mantle (Gao et al., 2002; Wu et al., 2003, 2006).

The age of the CLM in the Yangtze craton *prior to* the Triassic is unknown. Reisberg et al. (2005) show that peridotite xenoliths carried in Cenozoic basalt from the Subei basin south of the Sulu terrane (Fig. 1), define correlations between Os isotopes and Yb and Al_2O_3, giving an intercept $^{187}Os/^{188}Os$ ratio of ~0.116, which corresponds to an age of around 1.8 Ga. However, it is difficult to constrain the nature of the pre-Triassic CLM of the Yangtze craton using the Subei samples. First, the Subei xenoliths are carried in Cenozoic basalt, which post-dates the Triassic collision and, like the eastern block of the NCC, the CLM of the Yangtze craton might also have changed significantly in the Mesozoic, as Jurassic and Cretaceous magmatism was also widespread there. Secondly, the Subei locality lies just north of the proposed location of the sub-surface suture zone between the Yangtze craton and the NCC, whose extension at depth is still controversial (Li, 1994; Chung, 1999; Faure et al., 2001).

Nevertheless, if we assume that the Dabie–Sulu belt formed by collision of the Yangtze craton with the *eastern block* of the NCC during the Triassic and that the Archean aged CLM of the latter persisted until the Triassic collision, the Paleoproterozoic ages of the Sulu peridotites preclude their derivation from the *adjacent* eastern block of the NCC in the Triassic. In contrast, derivation from the Yangtze craton is consistent with the existing tectonic model of the Dabie–Sulu belt and the Proterozoic ages of inherited zircons in the Dabie–Sulu eclogites and surrounding gneisses, as described above. We thus infer that, like the crustal eclogites and gneisses, the Dabie–Sulu mantle peridotites also derive from the subducted Yangtze plate and probably represent continental lithospheric mantle from this craton that formed in the Paleoproterozoic. The ancient Os ages also rule out their derivation from Triassic mantle wedge materials. Together with previous petrological studies of Dabie–Sulu mantle peridotites (Zhang et al., 2000, 2003; Zhang and Liou, 2003; Zhang et al., 2005), our results support the notion that the crust and underlying lithospheric mantle of the Yangtze craton were both subducted to depths of >180–200 km during the Triassic collision to form the world's largest Dabie–Sulu UHP belt.

Finally, Ying et al. (2006) recently described spinel lherzolite xenoliths from a Late Cretaceous (~67 Ma) basaltic breccia at Jünan that intrudes very near the outcrop of the Xugou peridotites in the Sulu terrain (Fig. 1). They note two types of peridotites: low Mg# peridotites (containing $Fo_{88–89}$ olivine and low Cr# spinel-8–19) and rarer, high Mg# peridotites (containing Fo_{92} olivine and moderate Cr# spinel-52). Although the single high Mg# peridotite they describe has an equilibration temperature on the high end of the range for the total suite, its temperature overlaps those of the low Mg# peridotites, so there is no obvious depth stratification on the basis of temperature. Ying et al. (2006) suggested that the rare, high Mg# peridotite xenolith may represent a relict of Archean-aged mantle lithosphere from the NCC that persisted beneath the Sulu terrane during the Late Mesozoic, in close proximity to the low Mg# peridotites, which they infer to be newly accreted mantle lithosphere derived from the convecting mantle during the Cretaceous. Since the range of compositions in these xenoliths overlaps those of the Xugou peridotites, an alternative interpretation is that they form the lithospheric mantle of the Yangtze craton that was subducted beneath the NCC. The differences in the REE patterns between the Jünan xenoliths (which range from convex-upwards to LREE depleted) and the Xugou peridotites (which are generally LREE enriched) may reflect LREE addition to the latter that is inferred to have occurred shortly before their exhumation.

6. Conclusions

Whole-rock and mineral compositional data for the Xugou mantle peridotites from the Sulu terrane reflect variable degrees of melt extraction. Although these peridotites were strongly serpentinized and probably metasomatized with recent addition of REE and Re, the Re–Os systematics for the most refractory peridotites are largely intact. The T_{RD}, T_{MA} and errorchron ages yield similar results and suggest that timing of melt depletion was around 2.0 Ga. The ages are similar to available ages for mantle peridotites from the Dabie terrane, but are much younger than the Archean CLM ages beneath the adjacent eastern block of the NCC. If we assume that the

Dabie–Sulu belt formed by the Triassic collision of the Yangtze craton with the *eastern block* of the NCC and that the Archean aged CLM of the latter persisted until the Triassic, the Paleoproterozoic model ages suggest derivation of the Dabie–Sulu peridotites from the Yangtze craton. This is consistent with the existing tectonic model of the Dabie–Sulu UHP belt and ages of zircons in the Dabie–Sulu eclogites and surrounding gneisses. Our results suggest that, like the crustal eclogites and gneisses, the peridotites from the Dabie–Sulu UHP belt also derive from the Yangtze craton, and add further support that the crust and underlying lithospheric mantle of the Yangtze craton as a whole were subducted to depth of >180–200 km. Further work is needed to study possible modification of the CLM of the NCC during the Triassic collision and the age of the Yangtze CLM.

Acknowledgements

This work was supported by the National Natural Science Foundation of China (Grants 40521001, 40302015) and the Ministry of Education of China (Grants IRT0441 and 306021) to S. Gao and H.L. Yuan as well as NSF grant EAR 99031591 to R.L. Rudnick. We thank Hua Huang and Fangyue Wang for their help in sample preparation and electron microprobe analysis. We also thank H.F. Zhang for providing unpublished Re–Os data on peridotites from the kimberlites and J.-P. Zheng for sharing papers in press. The paper benefited from constructive comments of Laurie Reisberg and Ruth Zhang and discussion with J.-P. Zheng and the efficient editorial handling of Steve Goldstein.

References

Alard, O., Griffin, W.L., Lorand, J.P., Jackson, S.E., O'Reilly, S.Y., 2000. Non-chondritic distribution of the highly siderophile elements in mantle sulphides. Nature 407, 891–894.

Ames, L., Zhou, G.Z., Xiong, B.C., 1996. Geochronology and isotopic character of ultrahigh-pressure metamorphism with implications for the collision of the Sino–Korean and Yangtze cratons, central China. Tectonics 15, 472–489.

Ayers, J.C., Dunkle, S., Gao, S., Miller, C.F., 2002. Constraints on timing of peak and retrograde metamorphism in the Dabie Shan ultrahigh-pressure metamorphic belt, east-central China, using U–Th–Pb dating of zircon and monazite. Chem. Geol. 186, 315–331.

Bennett, V.C., Nutman, A.P., Esat, T.M., 2002. Constraints on mantle evolution from $^{187}Os/^{188}Os$ isotopic compositions of Archean ultramafic rocks from southern West Greenland (3.8 Ga) and Western Australia (3.46 Ga). Geochim. Cosmochim. Acta 66, 2615–2630.

Birck, J.L., Roy-Barman, M., Capmas, F., 1997. Re–Os isotopic measurements at the femtomole level in natural samples. Geostand. Newsl. 21, 19–27.

Bodinier, J.L., Godard, M., 2003. Orogenic, ophiolitic, and abyssal peridotites. In: Carlson, R.W. (Ed.), The Mantle and Core. In: Holland, H.D., Turekian, K.K. (Eds.), Treatise on Geochemistry, vol. 2. Elsevier–Pergamon, Oxford, pp. 103–170.

Carlson, R.W., Pearson, D., James, D.E., 2005. Physical, chemical, and chronological characteristics of continental mantle. Rev. Geophys. 43, RG1001. doi:10.1029/2004RG000156.

Chesley, J.T., Rudnick, R.L., Lee, C.T., 1999. Re–Os systematics of mantle xenoliths from the east African rift: age, structure, and history of the Tanzanian craton. Geochim. Cosmochim. Acta 63, 1203–1217.

Chung, S.-L., 1999. Trace element and isotope characteristics of Cenozoic basalts around the Tanlu fault with implications for the Eastern Plate Boundary between North and South China. J. Geol. 107, 301–312.

Cohen, A.S., Waters, F.G., 1996. Separation of osmium from geological materials by solvent extraction for analysis by TIMS. Anal. Chim. Acta 332, 269–275.

Faure, M., Lin, W., Le Breton, N., 2001. Where is the North China–South China block boundary in eastern China? Geology 29, 119–122.

Gao, S., Rudnick, R.L., Carlson, R.W., McDonough, W.F., Liu, Y.S., 2002. Re–Os evidence for replacement of ancient mantle lithosphere beneath the North China craton. Earth Planet. Sci. Lett. 198, 307–322.

Gao, S., Rudnick, R.L., Yuan, H.L., Liu, X.M., Liu, Y.S., Xu, W.L., Ling, W.L., Ayers, J., Wang, X.C., Wang, Q.H., 2004. Recycling lower continental crust in the North China Craton. Nature 432, 892–897.

Griffin, W.L., Zhang, A., O'Reilly, S.Y., Ryan, C.G., 1998. Phanerozoic evolution of the lithosphere beneath the Sino–Korean Craton. In: Flower, M., Chung, S.L., Lo, C.H., Lee, T.Y. (Eds.), Mantle Dynamics and Plate Interactions in East Asia. Geodynamics Series, vol. 27. American Geophysical Union, Washington, D.C., pp. 107–126.

Hacker, B.R., Ratschbacher, L., Webb, L., Ireland, T., Walker, D., Dong, S., 1998. U/Pb zircon ages constrain the architecture of the ultrahigh-pressure Qinling–Dabie Orogen, China. Earth Planet. Sci. Lett. 161, 215–230.

Hacker, B.R., Ratschbacher, L., Webb, L., McWilliams, M.O., Ireland, T., Calvet, A., Dong, S., Wenk, H.R., Chateigner, D., 2000. Exhumation of ultrahigh-pressure continental crust in east central China: Late Triassic–Early Jurassic tectonic unroofing. J. Geophys. Res. 105, 13339–13364.

Handler, M.R., Bennett, V.C., Esat, T.M., 1997. The persistence of off-cratonic lithospheric mantle: Os isotopic systematics of variably metasomatised southeast Australian xenoliths. Earth Planet. Sci. Lett. 151, 61–75.

Jahn, B.M., Fan, Q.C., Yang, J.J., Henin, O., 2003. Petrogenesis of the Maowu pyroxenite–eclogite body from the UHP metamorphic terrane of Dabieshan: chemical and isotopic constraints. Lithos 70, 243–267.

Jin, Y.B., Zhi, X.C., Meng, Q., Gao, T.S., Peng, Z.C., 2004. Re–Os dating of the Raobazhai ultramafic massif in North Dabie. Chin. Sci. Bull. 49, 508–513.

Lee, S.R., Walker, R.J., 2006. Re–Os isotope systematics of mantle xenoliths from South Korea: evidence for complex growth and loss of lithospheric mantle beneath East Asia. Chem. Geol. 231, 90–101.

Lee, C.-T., Yin, Q., Rudnick, R.L., Chesley, J.T., Jacobsen, S.B., 2000. Osmium isotopic evidence for Mesozoic removal of lithospheric mantle beneath the Sierra Nevada, California. Science 289, 1912–1916.

Li, Z.-X., 1994. Collision between the North and South China Blocks: a crustal-detachment model for the suturing in the region east of the Tanlu fault. Geology 22, 739–742.

Li, S., Xiao, Y., Liou, D., Chen, Y., Ge, N., Zhang, Z., Sun, S.-S., Cong, B., Zhang, R.Y., Hart, S.R., Wang, S., 1993. Collision of the North China and Yangtse blocks and formation of coesite-bearing eclogites: timing and processes. Chem. Geol. 109, 89–111.

Liou, J.G., Hacker, B.R., Zhang, R.Y., 2000. Into the forbidden zone. Science 287, 1215–1216.

Liu, F., Xu, Z., Xue, H., 2004. Tracing the protolith, UHP metamorphism, and exhumation ages of orthogneiss from the SW Sulu terrane (eastern China): SHRIMP U–Pb dating of mineral inclusion-bearing zircons. Lithos 78, 411–429.

Ludwig, K.R., 2003. User's Manual for Isoplot 3.0: a Geochronological Toolkit for Microsoft Excel Berkeley Geochronology Center Special Publication, vol. 4. 71 pp.

McDonough, W.F., Frey, F.A., 1989. Rare earth elements in upper mantle rocks. In: Lipin, B.R., McKay, G.A. (Eds.), Geochemistry and Mineralogy of Rare Earth Elements. Reviews in Mineralogy, vol. 21. Mineralogical Society of America, Washington, DC, pp. 100–145.

Meisel, T., Walker, R.J., Irving, A.J., Lorand, J.P., 2001. Osmium isotopic compositions of mantle xenoliths: a global perspective. Geochim. Cosmochim. Acta 65, 1311–1323.

Menzies, M.A., Fan, W.M., Zhang, M., 1993. Paleozoic and Cenozoic lithoprobes and the loss of >120 km of Archean lithosphere, Sino–Korean craton, China. In: Prichard, H.M., Alabaster, T., Harris, N.B.W., et al. (Eds.), Magmatic Processes and Plate Tectonics. Geol. Soc. Spec. Pub., London, pp. 71–81.

Morgan, J.W., 1985. Osmium isotope constraints on Earth's late accretionary history. Nature 317, 703–705.

Palme, H., O'Neill, H.St.C., 2003. Cosmochemical estimates of mantle composition. In: Carlson, R.W. (Ed.), The Mantle and Core. In: Holland, H.D., Turekian, K.K. (Eds.), Treatise on Geochemistry, vol. 2. Elsevier–Pergamon, Oxford, pp. 1–38.

Pearson, D.G., 1999. The age of continental roots. Lithos 48, 171–194.

Pearson, D.G., Canil, D., Shirey, S.B., 2003. Mantle samples included in volcanic rocks: xenoliths and diamonds. In: Carlson, R.W. (Ed.), The Mantle and Core. In: Holland, H.D., Turekian, K.K. (Eds.), Treatise on Geochemistry, vol. 2. Elsevier–Pergamon, Oxford, pp. 171–275.

Puchtel, I.S., Humayun, M., Walker, R.J., submitted for publication. Os–Pb–Nd isotope and highly siderophile and lithophile trace element systematics of komatiitic rocks from the Volotsk suite, SE Baltic Shield. Precambrian Research.

Reisberg, L., Lorand, J.P., 1995. Longevity of sub-continental mantle lithosphere from osmium isotope systematics in orogenic peridotite massifs. Nature 376, 159–162.

Reisberg, L., Lorand, J.P., Bedini, R.M., 2004. Reliability of Os model ages in pervasively metasomatized continental mantle lithosphere: a case study of Sidamo spinel peridotite xenoliths (East African Rift, Ethiopia). Chem. Geol. 208, 119–140.

Reisberg, L., Zhi, X.C., Lorand, J.P., Wagner, C., Peng, Z.C., Zimmermann, C., 2005. Re–Os and S systematics of spinel peridotite xenoliths from east central China: evidence for contrasting effects of melt percolation. Earth Planet. Sci. Lett. 239, 286–308.

Rudnick, R., Gao, S., 2003. Composition of the continental crust. In: Rudnick, R.L. (Ed.), The Crust. In: Holland, H.D., Turekian, K.K. (Eds.), Treatise on Geochemistry, vol. 3. Elsevier–Pergamon, Oxford, pp. 1–64.

Rudnick, R., Gao, S., Ling, W.L., Liu, Y.S., McDonough, W.F., 2004. Petrology and geochemistry of spinel peridotite xenoliths from Hannuoba and Qixia, North China craton. Lithos 77, 609–637.

Shirey, S.B., Walker, R.J., 1998. The Re–Os isotope system in cosmochemistry and high-temperature geochemistry. Annu. Rev. Earth Planet. Sci. 26, 423–500.

Taylor, S.R., McLennan, S.M., 1985. The Continental Crust: Its Composition and Evolution. Blackwell, Oxford, pp. 1–312.

Walker, R.J., Carlson, R.W., Shirey, S.B., Boyd, F.R., 1989. Os, Sr, Nd, and Pb isotope systematics of southern African peridotite xenoliths: implications for the chemical evolution of subcontinental mantle. Geochim. Cosmochim. Acta 53, 1583–1595.

Walker, R.J., Prichard, H.M., Ishiwatari, A., Pimentel, M., 2002. The osmium isotopic composition of convecting upper mantle deduced from ophiolite chromites. Geochim. Cosmochim. Acta 66, 329–345.

Walker, R.J., Brandon, A.D., Bird, J.M., Piccoli, P.M., McDonough, W.F., Ash, R.D., 2005. ^{187}Os–^{186}Os systematics of Os–Ir–Ru alloy grains from southwestern Oregon. Earth Planet. Sci. Lett. 230, 211–226.

Wang, X.B., Yang, J.S., Chen, S.Y., Shi, R.D., 2005. Origin and structural nature of Raobozhai ultramafic rocks: a discussion. Acta Pet. Sin. 21, 1593–1608.

Wu, F.Y., Walker, R.J., Ren, X.W., Sun, D.Y., Zhou, X.H., 2003. Osmium isotopic constraints on the age of lithospheric mantle beneath northeastern China. Chem. Geol. 196, 107–129.

Wu, F.Y., Lin, J.Q., Wilde, S.A., Zhang, X.O., Yang, J.H., 2005. Nature and significance of the Early Cretaceous giant igneous event in eastern China. Earth Planet. Sci. Lett. 233, 103–119.

Wu, F.Y., Walker, R.J., Yang, Y.-H., Yuan, H.-L., Yang, J.-H., 2006. The chemical-temporal evolution of lithospheric mantle underlying the North China Craton. Geochim. Cosmochim. Acta 70, 5013–5034.

Xu, Y.G., 2001. Thermo-tectonic destruction of the Archean lithospheric keel beneath the Sino–Korean Craton in China: evidence, timing and mechanism. Phys. Chem. Earth, Part A Solid Earth Geod. 26, 747–757.

Yang, J.J., 2003. Relict edenite in a garnet lherzolite from the Chinese Sulu UHP metamorphic terrane: implications for metamorphic history. Am. Mineral. 88, 180–188.

Yang, J.J., Jahn, B.M., 2000. Deep subduction of mantle-derived garnet peridotites from the Su-Lu UHP metamorphic terrane in China. J. Metamorph. Geol. 18, 167–180.

Ye, K., Cong, B.L., Ye, D.N., 2000a. The possible subduction of continental material to depths greater than 200 km. Nature 407, 734–736.

Ye, K., Yao, Y., Katayama, Y., Cong, B., Wang, Q., Maruyama, S., 2000b. Large areal extent of ultrahigh-pressure metamorphism in the Sulu ultrahigh-pressure terrane of East China: new implications from coesite and omphacite inclusions in zircon of granitic gneiss. Lithos 52, 157–164.

Ying, J.F., Zhang, H.F., Kita, N., Morishita, Y., Shimoda, G., 2006. Nature and evolution of Late Cretaceous lithospheric mantle beneath the eastern North China Craton: constraints from petrology and geochemistry of peridotitic xenoliths from Jünan, Shandong Province, China. Earth Planet. Sci. Lett. 244, 622–638.

Zhang, R.Y., Liou, J.G., 1998. Dual origin of garnet peridotites of Dabie–Sulu UHP terrane, eastern-central China. Episodes 21, 229–234.

Zhang, R.Y., Liou, J.G., 2003. Clinopyroxenite from the Sulu ultrahigh-pressure terrane, eastern China: origin and evolution of garnet exsolution in clinopyroxene. Am. Mineral. 88, 1591–1600.

Zhang, R.Y., Liou, J.G., Cong, B., 1994. Petrogenesis of garnet-bearing ultramafic rocks and associated eclogites in the Sulu ultrahigh-pressure metamorphic terrane, China. J. Metamorph. Geol. 12, 169–186.

Zhang, R.Y., Liou, J.G., Cong, B.L., 1995a. Ultrahigh pressure metamorphosed talc-, magnesite- and Ti-clinohumite-bearing mafic–ultramafic complex, Dabie Mountains, east-central China. J. Petrol. 36, 1011–1037.

Zhang, R.Y., Hirajima, T., Banno, S., Cong, B., Liou, J.G., 1995b. Petrology of ultrahigh-pressure rocks from the southern Sulu region, eastern China. J. Metamorph. Geol. 13, 659–675.

Zhang, R.Y., Liou, J.G., Yang, J.S., Yui, T.F., 2000. Petrochemical constraints for dual origin of garnet peridotites from the Dabie–Sulu UHP terrane, eastern-central China. J. Metamorph. Geol. 18, 149–166.

Zhang, R.Y., Liou, J.G., Yang, J.S., Ye, K., 2003. Ultrahigh-pressure metamorphism in the forbidden zone: the Xugou garnet peridotite, Sulu terrane, eastern China. J. Metamorph. Geol. 21, 539–550.

Zhang, R.Y., Yang, J.S., Wooden, J.L., Liou, J.G., Li, T.F., 2005. U–Pb SHRIMP geochronology of zircon in garnet peridotite from the Sulu UHP terrane, China: implications for mantle metasomatism and subduction-zone UHP metamorphism. Earth Planet. Sci. Lett. 237, 729–743.

Zhang, H.F., Goldstein, S.L., Zhou, X.H., Sun, M., 2006. Antiquity of sub-continental lithospheric mantle beneath the North China Craton: Re–Os isotopic reappraisal. Abstracts for International Conference on Continental Volcanism IAVCEI, p. 17.

Zhao, G.C., Wilde, S.A., Cawood, P.A., Sun, M., 2001. Archean blocks and their boundaries in the North China Craton: lithological, geochemical, structural and P–T path constraints and tectonic evolution. Precambrian Res. 107, 45–73.

Zheng, Y.F., Fu, B., Gong, B., Li, L., 2003. Stable isotope geochemistry of ultrahigh-pressure metamorphic rocks from the Dabie–Sulu orogen in China: implications for geodynamics and fluid regime. Earth-Sci. Rev. 62, 105–161.

Zheng, J.P., Zhang, R.Y., Griffin, W.L., Liou, J.G., O'Reilly, S.Y., 2005. Heterogeneous and metasomatized mantle recorded by trace elements in minerals of the Donghai garnet peridotites, Sulu UHP terrane, China. Chem. Geol. 221, 243–259.

Zheng, J.P., Griffin, W.L., O'Reilly, S.Y., Yang, J.S., Zhang, R.Y., 2006a. A refractory mantle protolith in younger continental crust, east-central China: age and composition of zircon in the Sulu ultrahigh-pressure peridotite. Geology 34, 705–708.

Zheng, J.P., Griffin, W.L., O'Reilly, S.Y., Zhang, M., Pearson, N., 2006b. Zircons in mantle xenoliths record the Triassic Yangtze–North China continental collision. Earth Planet. Sci. Lett. 247, 130–142.

Zheng, J.P., Griffin, W.L., O'Reilly, S.Y., Yang, J.S., Li, T.F., Zhang, M., Zhang, R.Y., Liou, J.G., 2006c. Mineral chemistry of peridotites from Paleozoic, Mesozoic and Cenozoic lithosphere: constraints on mantle evolution beneath Eastern China. J. Petrol. 47, 2233–2256.

Zhi, X.C., Jin, Y.B., Meng, Q., Gao, T.S., 2004. Trace element geochemistry of Raobazhai ultramafic complex, North Dabie Mountain. Acta Pet. Sin. 20, 463–472.